Three-dimensional simulation of void migration at the interface between thin metallic film and dielectric under electromigration

T. V. Zaporozhets,[a] A. M. Gusak,[b] and K. N. Tu[c]
Department of Materials Science and Engineering, University of California, Los Angeles, Los Angeles, California 90095-1595

S. G. Mhaisalkar
School of Materials Engineering, Nanyang Technological University, Singapore 639798, Singapore

(Received 20 December 2004; accepted 7 October 2005; published online 18 November 2005)

A kinetic Monte Carlo simulation of the electromigration-induced void migration behavior of three-dimensional nanovoids at the interface between a metal conductor and its dielectric overlayer is presented. Major stages of the recently observed failure mode of surface void migration and accumulation at the cathode via of Cu damascene interconnects were simulated, including the trapping at and detachment from grain boundaries (GBs) and GB triple junctions. The migration and shape evolution of voids along the interface and along the grain boundaries intersecting this interface have also been investigated in detail. The main results of the simulation correlate well with *in situ* observations as well as with simple analytical models of void trapping and detachment from GBs and their junctions. © *2005 American Institute of Physics*. [DOI: 10.1063/1.2131204]

I. INTRODUCTION

Nucleation and growth of voids induced by electromigration in Al lines has been one of the key reliability failure modes in microelectronics.[1–10] According to Huntington's mechanism of electromigration, the electron wind force generates a vacancy flux towards the cathode, where a sufficient supersaturation of vacancies can be reached, resulting in void nucleation, growth, and eventually failure at the cathode.[2,3] Recent experimental observations[4] have shown that in Cu dual-damascene structures, the void formation occurs on the surface of the interconnect. Furthermore, void nucleation may occur far away from the cathode, which is typically the eventual location of failure. It has also been reported that the surface voids may nucleate at defect sites in the middle of the Cu interconnects. Then driven by the electron wind force, the voids may coalesce with other voids, temporarily stop at defects such as grain boundary (GB) triple junctions, detach from these triple junctions, migrate further to reach the cathode via, and finally grow to large enough sizes leading to eventual open circuit failures.

Thus, migration and coalescence of voids as well as their interactions with GBs in the presence of the electric wind force is crucial for understanding the failure mechanism in Cu interconnects. The first fundamental theory of void (or other inclusions') migration under the electron wind force was developed by Krivoglaz and Osinowskiy[5] for an isolated spherical void and was later modified by Ho[6] for voids in the vicinity of an external surface. In the above treatment, the theory of electron wind force (Huntington and Crone[7] and Fiks[8]) was used to demonstrate a $1/R$ size dependence of void velocity. However, the interaction of a void with GBs during electromigration (EM) was not considered.

In this paper, *in situ* scanning electron microscopy (SEM) observations[4] of high current-density-induced nucleation, migration, and coalescence of voids on the surface of Cu interconnects or at the Cu/dielectric overlayer interface (Fig. 1) have been modeled by means of analytical treatments and computer simulations. In the simulation, a thin rectangular conducting film, up to 1 μm wide $\times$ 0.5 μm thick, surrounded by nonconducting material, was subjected to current densities of up to 10^{10}–10^{11} A/m^2. The two structures considered, namely M-1 and M-2 structures, are presented in Figs. 2(a) and 2(b), respectively. The M-1 structure corresponds to the experimental situation shown in Fig. 1 where the voids nucleate somewhere "in the middle" of the Cu/dielectric interface and migrate towards the cathode via opposite to the electron wind force instead of nucleating and growing directly at the via which is the location of the highest current density and the highest vacancy flux divergence. In the M-2 test structure [Fig. 2(b)] it was also observed that void nucleation occurs at the Cu/dielectric interface away from the via and migrates along this interface towards the corner above the via. It should also be noted that void nucleation and/or migration was not observed at the Ta/dielectric cap layer interface. Contrary to expectations, *in situ* experi-

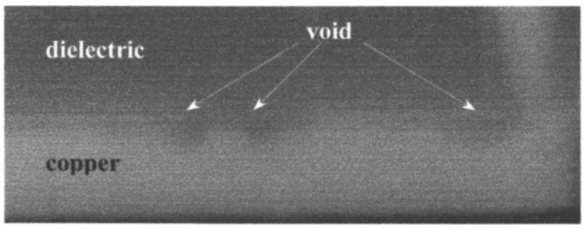

FIG. 1. Coalescence of voids at the interface between thin metallic (copper) and dielectric (*in situ*) films.

[a]On leave from Cherkasy National University, Ukraine; electronic mail: tvz@phys.cdu.edu.ua
[b]On leave from Cherkasy National University, Ukraine.
[c]Electronic mail: kntu@ucla.edu

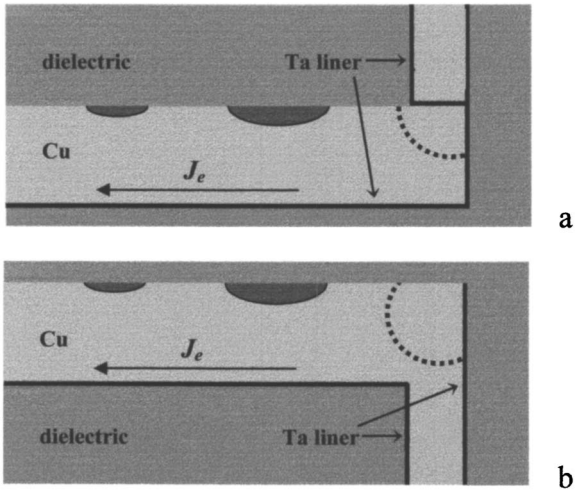

FIG. 2. Schematic of void migration in the lower layer M-1 (a) and the upper layer M-2 (b) structures (Ref. 4). In the M-2 line the void first emerged at Cu/dielectric interface at some distance from the via corner. It continued to grow and move along the Cu/dielectric interface towards the via corner at the cathode end of the line. Finally, the void agglomerated at the top corner of the M-2 line and its further growth towards the via caused failure. In the case of the M-1 structure, the void also nucleated at the Cu/dielectric interface at a considerable distance from the via and moved along this interface towards the via. Places of eventual void agglomeration are indicated with dotted lines.

mental observations on M-1 and M-2 structures indicate that void growth takes place not in the regions of high current density but in regions of low current density. A comprehensive understanding of void nucleation and migration is crucial for robust designs which are resistant to EM failures. In this study, EM-induced void migration along the metal/dielectric interface, with and without GBs, have been modeled. The simulations also included void trapping at GBs and at triple junctions. It should be noted that this investigation encompasses only a qualitative understanding of this process and accurate quantitative predictions have not been undertaken.

The possible shapes undertaken by the voids further complicate the problem under consideration. A change in the shape and/or position of a void leads to the redistribution of current and the corresponding drift terms, which in turn affects a further change in the shape of the void. Only two-dimensional (2D) schemes for solving such a coupled problem have been developed.[9] Applicability of 2D results obtained within phenomenological (continuous) models, to practical three-dimensional (3D) voiding in Cu interconnects, is at best questionable. This paper therefore undertakes to simulate the behavior of nanovoids under electron current using a 3D atomic Monte Carlo model[10] of a face-centered-cubic (fcc) crystalline material with and without GBs.

II. OVERVIEW OF CURRENT-INDUCED VOID EVOLUTION

The 3D Monte Carlo model developed in this report was closely based on *in situ* SEM observations previously reported in Ref. 4:

(1) voids are formed at surface defects and are bounded by the dielectric overlayer;
(2) these surface voids migrate under the electron wind force (Fig. 2);
(3) migration velocity depends on the void size and on the presence of defects (in particular, GBs);
(4) surface voids can migrate from one GB to another, as well as *along* GBs. In the latter case, the velocity depends on the type of boundary and on the angle between the field and the GB/surface intersection;
(5) voids can be trapped by GBs and/or GB junctions (vertices of bamboo grains);
(6) void velocity depends on size as well as trapping at GBs and leads to collisions and coalescence of voids (typically, the larger the path traversed, the larger the void);
(7) detrapping of voids from GBs or vertices is possible only after reaching a critical size (for GB trapping);
(8) voids tend to stop at the corners above (or below) the via, then grow, thus resulting in a critical decrease in the effective interconnect cross section leading to eventual failure.

An initial semispherical void, under electric current, at the surface of a thin-film-confined dielectric is considered. The evolution of the void in the absence of bulk diffusion is governed by two forces: (a) the electron wind force that pushes and eventually redistributes the surface atoms, trying simultaneously to shift the void and change its shape, and (b) the surface tension of the void that tries to minimize the void surface energy. Thus, the atomic flux density along the moving surface of the void consists of two terms,[2]

$$J_{\mathrm{at}} = \frac{c_S D_S}{k_B T} Z_{\mathrm{ef}} e E_S - 2\Omega\gamma \frac{\partial k}{\partial S}, \tag{1}$$

where c_S is the atomic concentration of mobile surface atoms (adatoms), D_S is the corresponding diffusivity, Z_{ef} is the effective charge of jumping ions (in general, differing from the effective charge of ions in the bulk), e is the elementary charge, E_S is the tangential component of electric field, Ω is the atomic volume, γ is the surface tension, k is the local surface curvature equal to half of the sum of the inverse radii of curvature, and $\partial k/\partial S$ is the directional derivative along void surface.

Equation (1) has a very simple form, but represents a challenging formulation for calculation since the electric field E_S is determined by the local current density which depends on the void shape. To find the local current density, one should solve the Laplace equation for electric potential in the whole sample at each new time moment. Inhomogeneity of the surface current leads to a complicated redistribution of surface atoms and consequently to shape evolution and void migration. In our simulations the ratio of maximum and minimum current densities can reach two orders of magnitude in the case of a semispherical void as represented in Fig. 3(a).

A schematic representation of shape evolution is observed in Fig. 3(b). Since the current density and corresponding atomic surface flux from A to B is less than the current density and flux from B to C, the material will be "eroded"

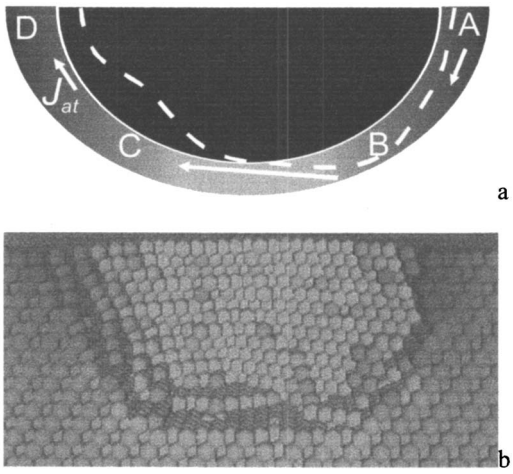

FIG. 3. Current density distribution around the void surface: (a) calculated in the frame of atomic MC model—brightness is proportional to current density, and (b) shape evolution of initially spherical void, caused by the current divergence.

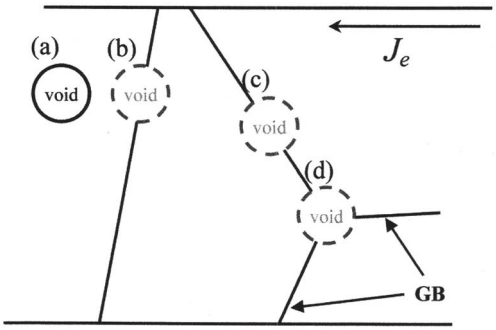

FIG. 4. Possible cases of void location at the dielectric/metal bamboo film interface (the schematic represents the top view of line): (a) at the metal/dielectric film interface, far from GBs; (b) interaction with the GB (transverse to the current direction as an extreme case), and the possibility of trapping at the GB and release from trap; (c) migration along GBs of different orientations with respect to the current; (d) possibility of trapping at a GB junction (vertices of thin-film grains).

and the void will extend in location B. On the other hand, since the current and the flux from B to C is larger than that from C to D, a material accumulation will be observed at location C.

Thus, a change in current density causes the motion of the void and also a change in the shape of the void. This in turn leads to a current redistribution in the new configuration. Thus, we have a self-consistent problem, that does not have an analytical solution. Furthermore, numeric modeling is meaningful only for a 3D case, since even for a semispherical void, a 2D projection (semicircle) does not provide the real picture of current and flux distribution.

III. MODEL

To model the shape evolution, atomic displacements in the frame of a stochastic Monte Carlo method, with probability of displacement that depends exponentially on the change of energy as a result of displacement, are considered:

(1) The metallic film material is modeled at an atomic level, in a Cu (fcc) lattice (lattice parameter $a=3.615$ Å). The external surface is considered to be a (111) plane and bulk diffusion is negligible.

(2) The energy of an atom consists of the effective energy of an ion in the field of the electron wind force $Z_{\mathrm{ef}}eU$ ($Z_{\mathrm{ef}}=38$, U is the electric potential; actually, we are interested only in the change of this "energy" that is equal to the work of the electron wind force during atomic displacement) plus the sum of pair interactions zE (z is number of nearest neighbors for surface atom, $0 \leqslant z \leqslant 12$, E is the pair interaction energy estimated from the sublimation energy of copper, $E=-0.587$ eV).

(3) The field of the electric potential U is determined at a grid, coinciding with the atomic fcc lattice. Instead of using the traditional finite element analysis, we use the finite difference method of solving the Laplace equation $\nabla(1/\rho\nabla U)=0$ for U with the following time-dependent boundary conditions: $\Delta U=\rho Jl$, with resistance $\rho=10^{-8}$ Ω m, the current density away from the void $J=10^{14}$ A/m^2 (reasons of such high current density will be discussed below), and l is the sample length.

(4) Since GBs seem to play an important role in void movement, the model constructed herein consists of several grains and grain boundaries, which are introduced artificially, by prescribing different values of interaction energies to atoms that make up the grain boundary, i.e., the interaction energies of atoms within each grain is identical, but the interaction energies of the atoms contained at the grain boundaries is different. Geometrically all grains are identical and employ a rigid 3D grid, a scheme that is customarily used in Monte Carlo (MC) modeling. The void behavior under the electron wind force is simulated for the following cases (see Fig. 4):

(a) at the metal/dielectric interface far from GBs;
(b) interaction with GBs (transverse to the current direction as an extreme case), and possibility of trapping at and release from GBs;
(c) migration along GBs with varied orientations with respect to the current;
(d) possibility of trapping at GB junctions (vertices of thin-film bamboolike grains).

(5) We distinguish the following sets of lattice sites which include empty sites inside a void as well as vacancies (Fig. 5): set {0}—dielectric; set {1}—atoms in the bulk of the first grain; set {2}—atoms in the bulk of the second grain; set {3}—atoms of the first grain, adjacent to set {−1}; set {4}—atoms of the second grain, adjacent to set {−1}; and set {−1}—empty sites (void and vacancies).

(6) Interactions between atoms belonging to the same or different sets may be described by a matrix of interaction coefficients $\Gamma=E_{ij}/E$ (i and j are set numbers), with parameters which are not well known and have been chosen from general physical considerations,

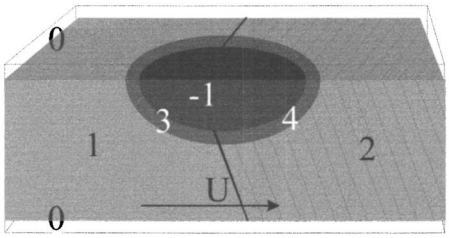

FIG. 5. Schematic of the modeled sample with two grains. Bias is applied to the left and right planar boundaries. In the other two directions, the sample is confined in the dielectric (0). Regions 1 and 2 correspond to the bulk of two different grains, 3 and 4 correspond to the surface atoms of these grains, neighboring with void (−1).

$$\begin{array}{c} set \\ -1 \\ 0 \\ 1 \\ 2 \\ 3 \\ 4 \end{array} \begin{array}{c} \begin{array}{cccccc} -1 & 0 & 1 & 2 & 3 & 4 \end{array} \\ \left(\begin{array}{cccccc} 0.0 & 0.0 & 0.0 & 0.0 & 0.0 & 0.0 \\ 0.0 & 0.0 & 0.5 & 0.5 & 0.5 & 0.5 \\ 0.0 & 0.5 & 1.0 & 0.4 & 1.0 & 0.4 \\ 0.0 & 0.5 & 0.4 & 1.0 & 0.4 & 1.0 \\ 0.0 & 0.5 & 1.0 & 0.4 & 1.0 & 0.4 \\ 0.0 & 0.5 & 0.4 & 1.0 & 0.4 & 1.0 \end{array} \right) \end{array} = \Gamma.$$

(7) Redistribution of the electric potential is recalculated for the actual configuration before and after the jump.
(8) Candidates for displacements are chosen only from the boundary sets {3,4}. The probability of displacement depends exponentially on the change of energy as a result of displacement.
(9) Displacement direction is chosen according to the residence time algorithm (RTA) with possible "jumps" of surface atoms (sets {3,4}) in empty sites (set {−1}) up to the nth coordination shell (in our case we took $n=7$).

Our initial attempts of EM-induced void migration simulations, at the above-mentioned experimental conditions and with using standard MC algorithms, demonstrated that the influence of the current remained practically unnoticeable for very long computational times. This can be understood based on the following discussion. For reasonable current densities of up to 10^{11} A/m^2 and an effective charge of about 38, the work of the electron wind force for one atomic displacement is less than 10^{-23} J. On the other hand, if an atomic jump leads to a change of nearest neighbors, at least by $\Delta z=1$, the change of energy is about 10^{-19} J. After optimization of the shape due to the surface tension, each surface atom has an optimal number of nearest neighbors. Furthermore, any change of configuration that leads to an increase of surface energy can be accepted with a reasonable probability only if the work of the electron wind force would compensate for this increase. However, as discussed above, the work of the electron wind force is actually four orders of magnitude smaller than that of the change in surface energy. Consequently, the observation of void migration by means of standard Monte Carlo (Metropolis algorithm with atomic jumps into empty sites within the first coordination sphere) simulations at reasonable current densities and nearest-neighbor jumps becomes practically unattainable.

Employing the RTA, where the jump would proceed irrespective of energy minimization, it is possible for the system to circumvent the above-mentioned limitations of the Metropolis algorithm. Once the energetically unfavorable transition into the first coordination shell is enabled, the system will proceed further via the conventional sequence of favorable and unfavorable configurations. Since the next MC step (MCS) usually deals with another surface atom, the back jumps which may restore the previous favorable configuration become highly improbable. Furthermore, the RTA algorithm with jumps only to the first coordination shell has led to another problem: generation of unfavorable higher energy configurations (with less number of neighbors for more and more surface atoms) may lead to a situation when the surface structure becomes fractal-like. The number of surface atoms with decreased number of neighbors grows exponentially; a situation that does not correspond to experimental observations (Fig. 6).

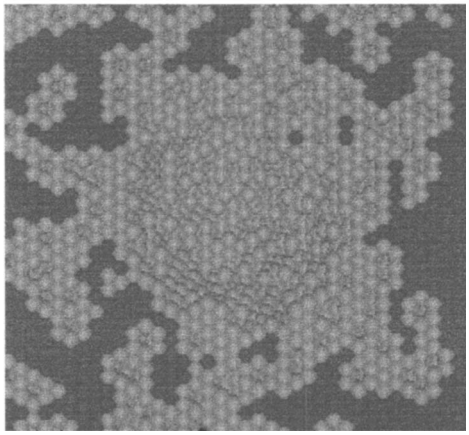

FIG. 6. Formation of fractal-like structure of empty sites in the case of the MC RTA algorithm with jumps into the first coordination shell (light atoms correspond to sets {3,4}, top view).

Time dependence of the bulk vacancy population, when allowing jumps only into the first coordination shell, shows a good fit with the parabolic law characteristic for random walk (see Fig. 7).

To circumvent the above-mentioned problems, jumps of the surface atoms up to nth coordination shell were allowed.

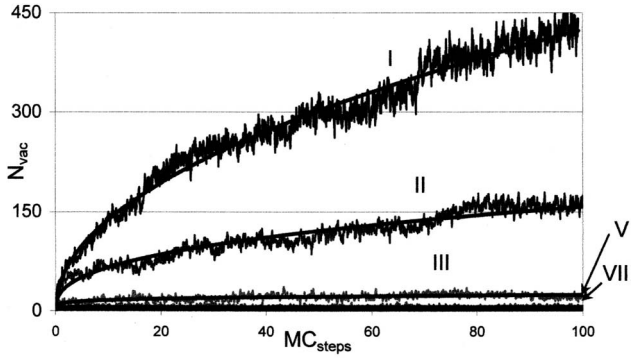

FIG. 7. Time dependence of the vacancy population in the bulk for a different number of coordination shells (I, II, III, V, VII) into which the "jumps" are allowed. Case I (jumps only into the first shell) shows parabolic multiplication of vacancies and corresponds to formation of fractal-like surfaces as seen in Fig. 6.

Thus, we broaden the spectrum of possible after-jump configurations, and therefore make the possibility of choosing the favorable configuration more probable. The larger is the n value, the less fractal-like is the surface as evident from the $n=5$ condition presented in Fig. 7. The seventh shell contains 35% of the total number of sites in the first seven shells and was thus included in this analysis. Actually, the notion of jump here means the series of elementary steps, after which the atom may find itself in the nth coordination shell. Such behavior of migrating atoms is in accordance with the complicated nature of surface diffusion, including a variety of different surface diffusion mechanisms.

Thus, our "double trick" (RTA for surface atoms plus jumps within the seventh shell) opens up more possibilities for atoms to shift under the electron wind force without changing the surface energy. This reduces the computational time required for overcoming unfavorable configurations and allows the system to experience the input of a weak electron wind without a huge number of MCS. Furthermore, it does not waste computational time for formation and disappearance of short-living unfavorable configurations and avoids formation of fractal-like surfaces.

All these approaches still did not sufficiently reduce the computation times, and therefore, similar to the approach taken by others,[9] larger current densities were used in this simulation.

IV. RESULTS

We investigate the motion of voids, with an initial semispherical shape, along the metal/dielectric interface. The motion of the void along the interface, with and without GBs and their junctions was simulated. To obtain some reference point for our results, we also simulated the motion of initially spherical voids in the bulk since an analytical solution for such a problem is available.[5,6] Faceting of the voids was observed in all simulations (see Fig. 8).

A. Migration of voids in bulk Cu and determination of the calibration factor between MCS and real time

Since each MCS of our scheme does not correspond to elementary atomic jump and may include a combination of different surface diffusion mechanisms, it is necessary to find the relationship (calibration factor) between MCS and real time. For this reason we simulated the migration of initially spherical voids in bulk Cu. According to published literature,[5,6] the velocity of the void (provided that the spherical shape is being preserved during migration), in the absence of volume diffusion, is determined by

$$v = \frac{dX}{dt_{\text{real}}} = \frac{Z_{\text{ef}} eJ}{k_B T} 3 D_S c_S \Omega \times \frac{1}{R}. \tag{2}$$

We simulated the voids with radii $4a$, $6a$, and $8a$, where a is the lattice parameter, with the above-mentioned model parameters. In accordance with analytical predictions, and despite the observed faceting, we observe that the velocity is inversely proportional to the void radius,

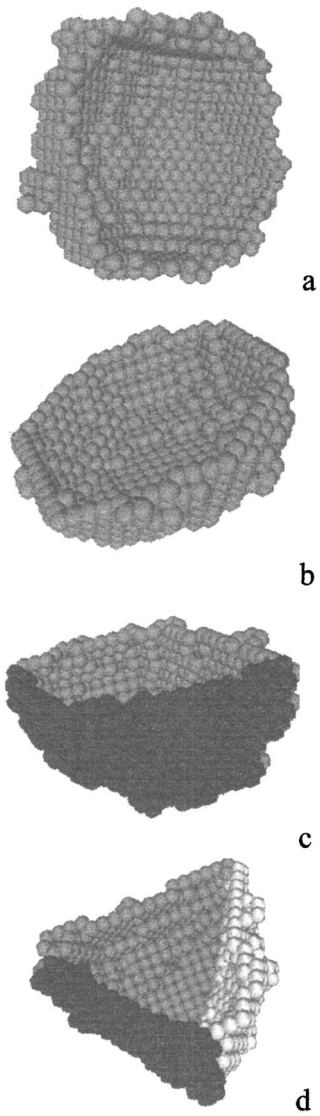

FIG. 8. Relaxed spherical void in the bulk and relaxed semispherical void at the metal/dielectric interface: (a) equatorial section of initially spherical void in the bulk; (b) initially semispherical void far from the GB; (c) initially semispherical void at the GB; (d) initially semispherical void at the triple junction of grains. Different colors correspond to surface atoms of different grains (sets {3,4}).

$$\tilde{v} = \frac{dX}{dt_{\text{MCS}}} = 6.181\,036 \times 10^{-21} \times \frac{1}{R} - 9.865871 \times 10^{-14}$$

with error up to 2.5%.

The constant in this equation is about 3.5% of the linear term for a radius of $6a$. So, we have neglected it for calibration. Using the above-mentioned parameters and neglecting the free term, we can rewrite the last equation in the form, similar to Eq. (2),

$$\tilde{v} = \frac{dX}{dt_{\text{MCS}}} \cong 0.594 \times \frac{Z_{\text{ef}} eJ}{k_B T} \Omega \frac{1}{R}. \tag{3}$$

Comparing Eqs. (2) and (3), we obtain the relation between real time and MCS time (in our simulations) in terms of surface diffusivity,

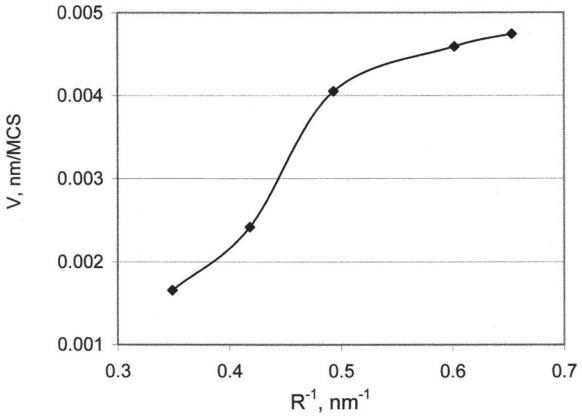

FIG. 9. Dependence of void velocity on void size (cubic root of volume) in the absence of GBs.

$$t_{\text{real}} = \frac{0.198}{D_S c_S} \times t_{\text{MCS}}. \tag{4}$$

B. Surface void migration along the interface metal/dielectric in the absence of GBs

We simulated an initially semispherical void containing 2505 empty sites at the interface between Cu and the capping layer. Besides faceting, voids also become nonequiaxial, more shallow, and elongated by about 10%–30% in the presence of electromigration. In such cases, Eq. (2) is inapplicable. The variation of void velocity with radius (cubic root of volume) was observed to be monotonically increasing, but was far from being linear (Fig. 9). Note that the nonlinear dependence was also reported for 2D voids of atomic thicknesses.[9]

C. Void migration along GBs of different orientations with respect to current

Owing to the minimization of surface energy, the surface voids prefer to be situated at the GB/capping layer interface. Therefore void migration along a grain boundary should also be studied. We investigated such migration for three cases:

(a) the limiting case of GB being parallel to the current direction ($\theta = \theta^\circ$);
(b) the limiting case of GB being perpendicular to the current direction ($\theta = 90^\circ$);
(c) some arbitrary angle between GB and current direction ($0^\circ \leqslant \theta \leqslant 90^\circ$).

When void migration takes place along a GB that is parallel to the current direction [case (a)], the void velocity was found to be 33% larger than the case when the void is far from the GB. One of the possible contributors may be the larger tangential component of the electric field E_S for the shallow elongated (boatlike) voids.

The interaction of surface voids with GBs perpendicular to the current direction [case (b)] demonstrates the following mechanism of trapping and detachment. After reaching the GB, the void changes its shape [Fig. 10(a)], holding on to the GB and simultaneously elongating towards the cathode [Fig. 10(b)], and forming a "fishlike" shape with an elongated "tail-like" structure [Fig. 10(c)]. The void eventually detaches from the GB leaving its tail at the GB [Fig. 10(d)]. In this simulation [case (b)], the tail (residual void) consists of 43 sites, whereas, the detached void consists of 944 sites. According to the simplified estimates given below in Sec. V, such void is overcritical and should indeed detach from the GB. Note that, according to our simulations, the surface void at GB can behave itself like a Frank-Reed dislocation source, continuously producing new voids under the influence of current and in the presence of vacancy supersaturation and migrating voids and vacancies.

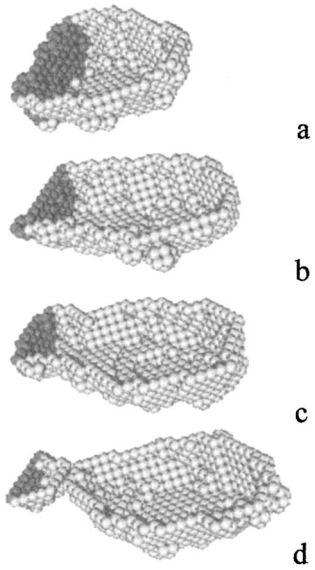

FIG. 10. Evolution of void detachment from GBs that are perpendicular to the current direction: (a) 0 MCS; (b) 466 MCS; (c) 701 MCS; and (d) 944 MCS.

In case (c), the void experiences two competing factors during its movement along the GB. At first, the projection of the current on the direction of the GB pushes the void along the GB. On the other hand, the projection of the current on the normal to the GB tries to detach the void from the GB. The outcome of this competition depends on the angle between the GB and the current. The critical angle depends on the current density and the surface tension (see Sec. VI).

As could be anticipated, the void velocity along the GB decreases with increasing angle. For example, for $\theta = 60^\circ$ the velocity is 40% of the velocity for $\theta = 0^\circ$. Similar to the case (b) when the GB is perpendicular to the current, the void in case (c) becomes fishlike with tail-like extension [Fig. 11(e)] and eventually detaches from the GB, leaving its tail at the GB [Fig. 11(f)]. The void shape appears to be nonsymmetric, influenced primarily by the angle the velocity makes with the GB [Fig. 11(d)]. In this case, the tail consists of 157 sites, whereas the original void consisted of 1746 sites. According to simplified estimates below in Sec. V, such void is also overcritical and should detach from the GB.

D. Behavior of the voids at triple junctions of GBs

From above we find that a GB, perpendicular to the current, may trap small voids migrating along the interface. This

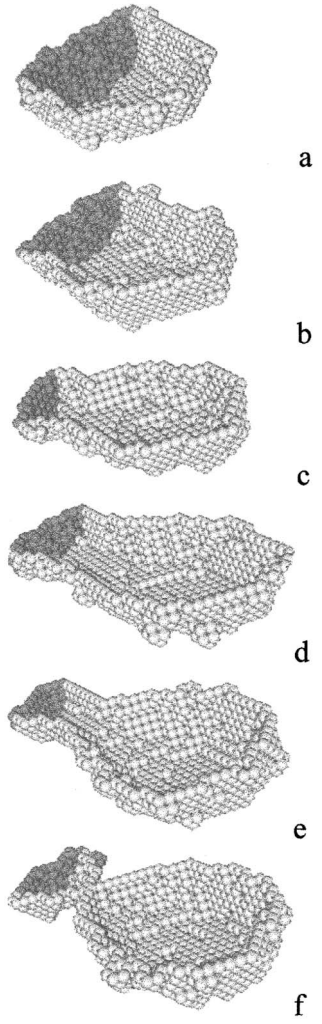

FIG. 11. Evolution of void detachment from GBs, forming an angle $\theta = 60°$ with the current direction: (a) 0 MCS; (b) 463 MCS; (c) 684 MCS; (d) 980 MCS; (e) 1227 MCS; and (f) 1277 MCS.

section addresses the interaction between voids and triple junctions of three GBs and metal surfaces. Herein we consider a triple junction of grains with identical surface tension (angles between grain boundaries are equal to 120°, $\theta = 0°$). Voids migrating along the GB, parallel to the current [Fig. 12(a)] make contact with the GB junction and undergo a shape evolution that can be described in the following stages:

- Upon reaching the GB junction, the void becomes deeper along the junction line and its velocity decreases [Fig. 12(b)];
- The current tries to push the void, whereas, the junction tries to trap it. Consequently, the void becomes triangular in shape, more or less symmetrical to both the GBs [Fig. 12(c)];
- Then the void has to choose either *one* of the GBs for propagation, and begins to move along the chosen GB [Fig. 12(d)];
- Subsequently, the void leaves the GB joint and migrates along the GB with an elongation along the current direction [Fig. 12(e)].

The time dependence of the distance between the center of the void and the GB junction, L, (Fig. 12) demonstrates

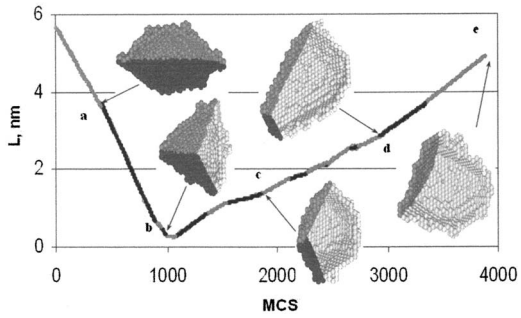

FIG. 12. Kinetics of the void motion in the vicinity of GB junctions. L is the distance between the void center and the GB junction; (a) as the void makes contact with the GB junction; (b) relaxed shape at the GB-junction; (c) the transition to a triangularly shaped symmetrical void under the current effect; (d) the crossover to a single GB (accompanied with a loss of symmetry); (e) the migration along the GB after detaching from the GB joint.

that the velocity of the void increases as the void approaches the GB junction (Fig. 12, interval a–b). Upon reaching the GB junction, the void virtually stops, deepens, before assuming a triangular symmetrical shape (Fig. 12, part b, plateau region). Subsequently, the void elongation leads to displacement and simultaneous trapping at the GB junction (Fig. 12, interval b–c). During the subsequent displacements and eventual motion along the one chosen GB, the void velocity (Fig. 12, interval d–e) is lower than the velocity during its approach path (Fig. 12, interval a–b), but higher than the void velocity during crossover from the junction to the single GB (Fig. 12, interval c–d).

The change in the shape of the void is important for the comprehension of the change in the void velocity as seen in Fig. 12(b). After touching the GB junction, the void becomes dipolelike, with its front part attached to the junction [Fig. 13(a)]. A relaxation at the GB junction follows, with the void acquiring a more symmetrical shape. This relaxation is thought to contribute to the delay observed in Fig. 12(b) and [Figs. 13(b)–13(d)]. Furthermore, the competition between the electron wind force and the reduction in the GB surface energy, due to the presence of the void, leads to oscillations in the void shape [Figs. 14(b)–14(d)] and a reduction in void velocity (Fig. 12, interval c–d).

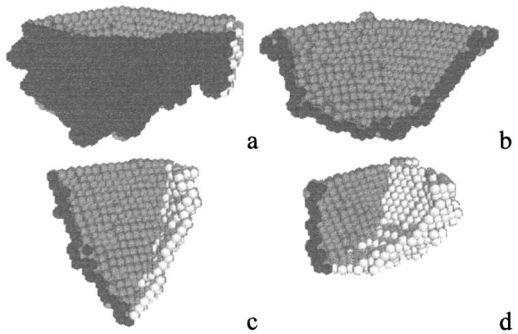

FIG. 13. Snapshots of void migration: (a) dipole like void approaching the GB junction (b)–(d) the cross sections of the void at time moments corresponding to stages (a)–(c) in Fig. 12, just before the crossover and just after passing the junction.

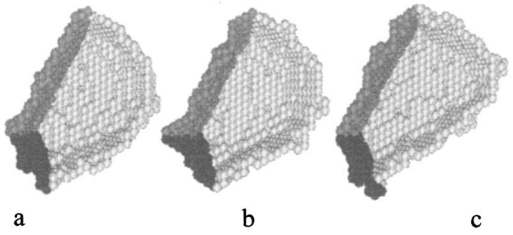

FIG. 14. Oscillations of the void shape before breaking up from the junction.

V. SIMPLIFIED ANALYTICAL MODELS OF TRAPPING AT THE GBS AND AT THE GB JUNCTIONS

According to the *in situ* observations described elsewhere,[4] migrating voids stop in certain locations (most probably GBs or their junctions), wait for ensuing voids, coalesce with them, grow in size, detach from the trapped sites, and subsequently continue towards the cathode. The simulation results described here were found to be in favorable agreement with experimental results. To better understand this phenomena, we propose herein two simplified models of the void trapping at GBs and at GB junctions.

A. Analytical model of trapping at a GB

We consider a semispherical void, of radius R, and situated initially symmetrically around the GB, at the surface making an angle θ with the direction of the current (Fig. 15). Under the electron wind force, this void will try to simultaneously move along the GB (increasing l) and to detach from the GB (increasing δ). Energetically, this process is determined by the competition of two factors. First, a motion at some sharp angle to the current direction leads to a decrease in electric energy (work of the electric field). Second, increasing δ means the increase in the grain-boundary surface area given by $(S_{\text{total}}-\pi R^2/2)-(S_{\text{total}}-\pi r^2/2)=\pi\delta^2/2$. If under the influence of the electron wind force, the void shifts a distance of $x_c=l\cos\theta+\delta\sin\theta$ along the electric field without change of shape, the system energy change can be expressed as

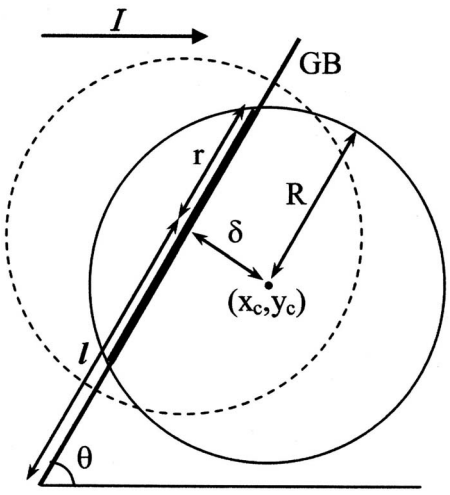

FIG. 15. Scheme of a semispherical void trapped at a GB, making an angle θ with the current direction.

TABLE I. Critical parameters of the void at the GB.

	θ	ρJ (V/m)	R^* (nm)	Number of empty sites
Realistic current conditions	90°	4×10^2	60.35	
Realistic current conditions	60°	4×10^2	64.85	
Model system	90°	1×10^6	1.21	311
Model system	60°	1×10^6	1.30	387

$$W^{\text{el}} = -Z_{\text{ef}}e\rho J\frac{2\pi}{3\Omega}R^3x_c + \pi\gamma\frac{\delta^2}{2}. \tag{5}$$

Substitution of x_c makes it possible to represent the energy change as the sum of two additive terms, indicating that the shift along the GB and the detachment from the GB are independent events:

$$W^{\text{el}} = \underbrace{-Z_{\text{ef}}e\rho J\frac{2\pi}{3\Omega}R^3\times l\cos\theta}_{W^{\text{el}}(l)} \underbrace{-Z_{\text{ef}}e\rho J\frac{2\pi}{3\Omega}R^3\times\delta\sin\theta+\pi\gamma\frac{\delta^2}{2}}_{W^{\text{el}}(\delta)}$$

The minimum of this dependence ($\partial W/\partial\delta=0$) determines the optimal (equilibrium) shift,

$$\delta^* = -\frac{2Z_{\text{ef}}e\rho JR^3\sin\theta}{3\gamma\Omega}. \tag{7}$$

If $\delta^*/R\geqslant 1$, the void will detach from the GB and will migrate further. By using this expression and rearranging the terms in Eq. (7), one can express the critical radius as

$$R^*_{GB} = \sqrt{\frac{3\gamma\Omega}{2Z_{\text{ef}}e\rho J}\times\frac{1}{\sin\theta}}. \tag{8}$$

The void trapped at a GB loses stability if it becomes larger than R^*. This may happen due to coalescence with other migrating voids or due to the consumption of vacancies. The lesser the θ and/or current density, the larger is the critical size for detachment. It should be noted that this is a simplified model since the inevitable shape changes of the void have not been considered.

Estimates of the critical size are presented in Table I for model parameters and realistic current densities for GB-current orientations of $\theta=90°$ and $\theta=60°$ ($\gamma=0.5$ J/m^2, $Z_{\text{ef}}=38$, $\Omega=1.18\times10^{-29}$ m^3).

Based on the estimation in this section, we can say that the voids simulated in MC, with 944 (case $\theta=90°$) and 1589 (case $\theta=60°$) sites, were overcritical and would spontaneously detach from the grain boundaries.

B. Analytical model of trapping at a GB junction

We consider a semispherical void, of radius R, and situated initially symmetrically around the GB junction, at the surface making an angle θ with the direction of the current (Fig. 16). When the void leaves the GB joint along one of the two GBs (GB_3), the surface and excess energy of the two remaining GBs (GB_1 and GB_2) increase (trapping factor), but

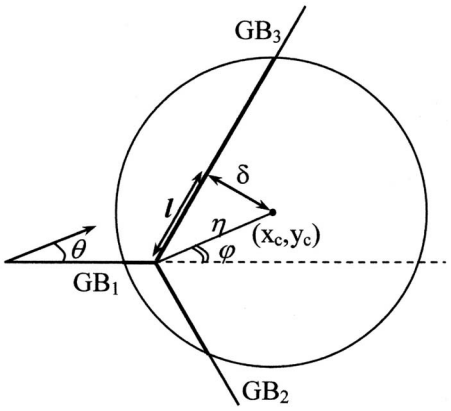

FIG. 16. Schematic of a semispherical void trapped at the GB junction making an angle θ with the current direction.

the surface and surface energy of GB_3 decreases, thus making it easier for the current to move the void. Assuming that the GBs forming the junction have the same surface tension, mechanical equilibrium implies that all angles between the GBs will be 120°. Let the current I be directed under some angle θ to GB_1. (In MC simulations this angle was zero.) Let δ be the distance between the center of the semispherical void and GB_3, and l be the distance between projection of this center on GB_3 and the joint position. Using polar coordinates η and φ, one can write $x_c=\eta\cos\varphi$, $y_c=\eta\sin\varphi$, $l=\eta\cos(\pi/3-\varphi)$, and $\delta=\eta\sin(\pi/3-\varphi)$. As discussed in Sec. V A, the critical void size for detrapping will depend upon the work of the electric current and the surface energy changes. In the present case the surface term includes three terms: $S^{GB}=S_0^{GB}-(S_1+S_2+S_3)$. Here S_0^{GB} is a total surface area of all the three grain boundaries in absence of the void. S_1, S_2, and S_3 are the areas of intersections of the void with the respective GBs. Interaction with the electric field is as described in Sec. V A: if the void center shifts from the junction position (x_0,y_0) to a new position (x_c,y_c) without a change in void shape, the system energy change due to the work of the electric field may be expressed as

$$W^{el}=-Z_{ef}e\rho J\frac{2\pi}{3\Omega}R^3\times\eta\cos(\varphi-\theta). \tag{9}$$

Thus, the total energy dependence on void position is

$$E(\rho,\varphi)=\text{const}-\gamma(S_1+S_2+S_3)-Z_{ef}e\rho J\frac{2\pi}{3\Omega}R^2\eta\cos(\varphi-\theta). \tag{10}$$

Here

$$S_i=\frac{r_i^2}{2}\left[\arccos\left(1-\frac{a_i}{r_i}\right)-\left(1-\frac{a_i}{r_i}\right)\sqrt{1-\left(1-\frac{a_i}{r_i}\right)^2}\right],\quad i=1,2,3, \tag{11}$$

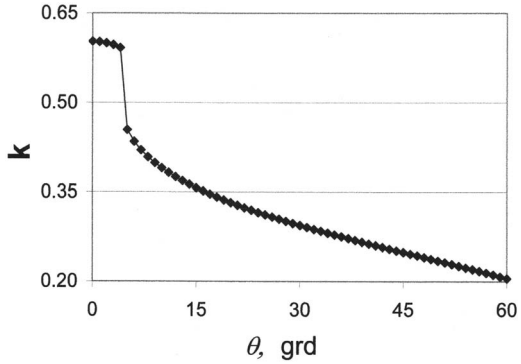

FIG. 17. Determination of $k(\theta)$ in Eq. (13).

$$r_1=\sqrt{R^2-\eta^2\sin^2\varphi},\quad a_1=r_1-\eta\cos\varphi,$$
$$r_2=\sqrt{R^2-\eta^2\sin^2\left(\frac{\pi}{3}+\varphi\right)},\quad a_2=r_2+\eta\cos\left(\frac{\pi}{3}+\varphi\right),$$
$$r_3=\sqrt{R^2-\eta^2\sin^2\left(\frac{\pi}{3}-\varphi\right)},\quad a_3=r_3+\eta\cos\left(\frac{\pi}{3}-\varphi\right). \tag{12}$$

Analysis of dependence of Eq. (10) demonstrates the existence of a critical size for voids to detach from the GB joint,

$$R^*_{\text{joint}}=k(\theta)\sqrt{\frac{3\gamma\Omega}{2Z_{ef}e\rho J}}, \tag{13}$$

where $k(\theta)$ depends on the angle between the direction of the current and GB_1. Numeric minimization procedures yield the coefficient $k(\theta)=0.6023$ when $\theta=0$ (Fig. 17).

VI. DISCUSSION

Our simulation and simplified analytical models demonstrate that the surface voids prefer to migrate along GBs. GBs with high angle with respect to current direction and triple GB junctions can slow down the movement even for voids of overcritical size [Eqs. (8) and (13)]. Undercritical sized voids can move along inclined GBs or grow in size by consuming the vacancy flux and/or ensuing voids. After reaching an overcritical size, the void detaches from the traps (GB or GB junctions). After detachment from GBs the voids leave behind residual voids at the GBs they detach from. It would be interesting to experimentally determine whether small residual voids can be detected at GBs after the detachment of a large void. In other words, a behavior analogous to a "Frank-Read-like void source" under electromigration stress may be observed.

The proposed analytical and numerical models, respectively, include simplifications such as neglecting the shape evolution and the use of very high current densities. Yet, these models seem to describe qualitatively the main features of *in situ* observations.[4] Thus, it may be claimed that the proposed mechanism of failure (Sec. II) is indeed probable.

Although our rough estimations of the critical void size of detachment by the simplified models with fixed shape seem to be reasonable, the kinetics of trapping and detachment cannot be predicted by these models. The most evident

example is the following. Consider a case of a semispherical void being trapped at a GB junction, with, for example, $\theta = 0$. If this semispherical void now detaches from the junction, it does not necessarily imply that the void becomes really free. It still intersects two GBs (2 and 3 at Fig. 16), and should try to detach from at least one of them, in order to move further. We did not describe this process in the framework of our analytical model since it would be energetically more favorable to optimize its shape so as to remain in contact with the GB junction.

Our results are in favorable agreement with the experimental behavior of voids in M-1 and M-2 structures (see Fig. 2). In the M-1 structure, the voids travel directly to the via, since they are to travel along the Cu/dielectric interface. In the M-2 structure, the Cu/dielectric interface is not connected to the via, and voids travel along this interface and agglomerate at the corner above the via prior to subsequent growth that leads to eventual via failure.

VII. CONCLUSIONS

(1) A simplified algorithm for MC simulations of void migration provides a reasonable description of this process in surface diffusion.
(2) In bulk diffusion, void velocity is observed to be inversely proportional with the void size. The dependence of velocity on the size for surface voids remains monotonically increasing, but is no longer linear. This may be considered to be the manifestation of the complex shape evolution and the corresponding changes in current distribution around the void. Therefore, we are not able to extrapolate the observed size dependence of velocity to dimensions in the range of 100 nm and larger.
(3) Small (undercritical) surface voids can be trapped at GBs. A rough criterion of trapping is given by Eq. (8). Detachment of overcritical voids from GBs proceeds with the formation of "fishlike" voids with an elongated "tail-like" structure, and tends to leave behind a small residual void at the GB.
(4) A GB junction is also a possible trap of voids [Eq. (13)]. Contrary to detachment from a single GB, detachment from the GB junction did not lead to formation of residual voids.
(5) Voids migrate faster along the GB/interface line than along the bulk/interface regions.

ACKNOWLEDGMENTS

This work was supported by CRDF Grant No. (UE1-2523-CK-09) and (in part) by Ministry of Education and Science of the Ukraine. Two of the authors (T.Z. and A.G.) are grateful to the Department of Materials Science and Engineering at UCLA for their hospitality.

[1] K. N. Tu, J. W. Mayer, and L. C. Feldman, *Electronic Thin Film Science* (Macmillan, New York, 1992).
[2] E. Artz, O. Kraft, W. D. Nix, and J. E. Sanchez, J. Appl. Phys. **76**, 1563 (1994).
[3] W. Wang, Z. Suo, and T.-H. Hao, J. Appl. Phys. **79**, 2394 (1996).
[4] A. V. Vairagar, A. Krishnamoorthy, K. N. Tu, S. G. Mhaisalkar, A. M. Gusak, and M. A. Meyer, Appl. Phys. Lett. **85**, 2502 (2004).
[5] M. A. Krivoglaz and M. Ye. Osinowskiy, Phys. Met. Metallogr. **24**, 36 (1967).
[6] P. S. Ho, J. Appl. Phys. **41**, 64 (1970).
[7] H. B. Huntington and A. R. Crone, J. Phys. Chem. Solids **20**, 76 (1961).
[8] V. B. Fiks, Sov. Phys. Solid State **3**, 16 (1959).
[9] H. Mehl, O. Biham, O. Millo, and M. Karimi, Phys. Rev. B **61**, 4975 (2000).
[10] K. N. Tu, J. Appl. Phys. **94**, 5451 (2003).